Isomerization of Indole. Quantum Chemical Calculations and Kinetic Modeling

Faina Dubnikova and Assa Lifshitz*

Department of Physical Chemistry, The Hebrew University of Jerusalem, Jerusalem 91904, Israel

Received: October 31, 2000; In Final Form: January 16, 2001

Density functional theory calculations were carried out to investigate the pathways of the unimolecular isomerizations of indole. Equilibrium and transition-state structures were optimized by the Lee−Yang−Parr correlation functional approximation (B3LYP) using the Dunning correlation-consistent polarized double-ξ basis set. Energy values were calculated at the CCSD(T) level of theory. Rate parameters for all the steps on the surfaces of the indole isomerizations were evaluated using B3LYP frequencies and CCSD(T)//B3LYP energy values. 3*H*-Indole, which is a stable tautomer of indole, is a precursor in the formation of *o*-tolyl isocyanide that by −NC → −CN flip forms *o*-tolunitrile. The latter is one of the isomers of indole. A second isomer, phenylacetonitrile, is obtained directly from indole. A kinetics scheme containing all the elementary steps on the surfaces was constructed, apparent rate constants for product formation were calculated, and comparison with experimentally available formation rates was made. The agreement for phenylacetonitrile is excellent. For *o*-tolunitrile the calculations somewhat underestimate the rate. Despite many efforts, a reaction path for the formation of *m*-tolunitrile based on indole as a starting point could not be calculated with activation energies compatible with the experimental findings. On the other hand, a reaction path for the isomerization starting from indole radical, with low-lying transition states and intermediates, was calculated. It is therefore suggested that indole radicals that are formed by various abstraction reactions are involved in the isomerization of indole to *m*-tolunitrile.

I. Introduction

Indole is the five-membered pyrrole ring fused to benzene. In both pyrrole and indole, isomerizations are the main thermal reactions.[1−3] Whereas the isomerization reactions of pyrrole have

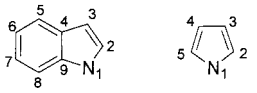

indole pyrrole

been extensively studied both experimentally and theoretically,[2−6] there is only one detailed experimental investigation on the thermal reactions of indole.[1] Pyrrole yields upon isomerization *cis*-crotonitrile, *trans*-crotonitrile, and vinylacetonitrile. It has been suggested[2,3] that the first step in all the three isomerization processes is tautomerization to 2*H*-pyrrole (pyrrolenine), which then isomerizes to the above-mentioned three isomers. This suggestion has been verified by a number of quantum chemical calculations, and a very good agreement between the experimental results and the calculations was obtained.[4,6]

The isomerization products of indole are phenylacetonitrile (vinylacetonitrile fused to benzene) and *o*-tolunitrile (*cis*-crotonitrile fused to benzene) and its *meta*-isomer.

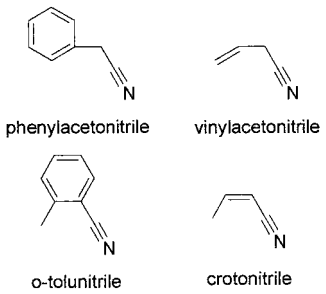

phenylacetonitrile vinylacetonitrile

o-tolunitrile crotonitrile

It has been shown that the active site of indole is C(3) and the most stable tautomer is 3*H*-indole (indolenine) in contrast to pyrrole, where the active site is C(2) and the stable tautomer is 2*H*-pyrrole.[1] 3*H*-Indole was identified spectoscopically in aqueous solutions, and its derivatives have been isolated.[7] It has thus been suggested that indole undergoes tautomerization to 3*H*-indole (indolenine) before isomerizing to *o*- and *m*-tolunitrile. Isomerization to phenylacetonitrile, on the other hand, can be very well rationalized as proceeding from both indole and 3*H*-indole.[1]

3H-indole

There are several quantum chemical calculations on the structure of indole[8−10] and its tautomerization to 3*H*-indole.[11] When this work was in progress, a paper by Zhou and Liu[12] on the isomerization of indole came to our attention. These authors calculated critical points on the indole isomerization potential energy surface using the B3LYP/6-311++G(2d,2p)//B3LYP/6-31G** level. The results of their study, except for the isomerization indole → phenylacetonitrile, are similar to ours. However, we have also done a detailed CI calculation, calculated isomerization rate constants, and compared the calculations with the experimental results obtained using the single-pulse shock tube technique.[1]

II. Computational Methods

A. Quantum Chemical Calculations. We used the Becke three-parameter hybrid method[13] with the Lee−Yang−Parr correlation functional approximation[14] (B3LYP) and the Dunning correlation-consistent polarized valence double-ξ (cc-

10.1021/jp004038+ CCC: $20.00
Published on Web 03/15/2001

pVDZ) basis set.[15] This level of theory and the basis set used gave good results in the calculations of pyrrole isomerization.[6] In addition, the structural parameters of indole calculated using the B3LYP level of theory gave good agreement with experimentally measured parameters.[9,10]

Structure optimization of the reactant, products, and intermediates was done using the Berny geometry optimization algorithm.[16] For determining transition state structures, we also used the combined synchronous transit and quasi-Newton (STQN) method.[17] Higher level calculations were then made using these geometries.

All the calculations were performed without symmetry restrictions. Vibrational analyses were done at the same level of theory to characterize the optimized structures as local minima or transition states. Calculated vibrational frequencies and entropies (at the B3LYP level) were used to evaluate preexponential factors of the reactions under consideration. All the calculated frequencies as well as the zero-point energies (ZPEs) are of harmonic oscillators. The zero-point energies were scaled by the ZPE scaling factor of 0.9806, and the entropies were scaled by the entropy scaling factor of 1.0015.[18] The calculations of the intrinsic reaction coordinate (IRC) were done at the B3LYP level of theory with mass-weighted internal coordinates, to check whether the transition states under consideration connect the expected reactants and products. Only this coordinate system permits one to follow the steepest descent path.[19] We computed the IRC path with the same basis set as was used for the stationary point optimization.

A few points on the potential energy surface of phenylacetonitrile having a biradical character were localized by the unrestricted uB3LYP method using the guess wave function with the destruction $\alpha-\beta$ and spatial symmetry. We used an open-shell singlet approximation for the biradical structures. It should be mentioned that numerous recent studies indicate that the spin-unrestricted B3LYP method for geometry optimization of biradical transition states and intermediates, and for energy barriers on the surface, were in reasonable agreement with the results of the multireference or multiconfigurational calculations and the corresponding experimental data.[20−27]

Each optimized B3LYP structure was recalculated at a single-point coupled cluster, including both single and double substitutions with triple excitations (CCSD(T)).[28,29] CCSD(T) calculations were performed with the frozen core approximation. We have also examined the multireference character of the transition states and intermediates by determining values of T_1, a diagnostic that was introduced by Lee and Taylor to determine the degree of the multirefence character.[30] All species had a T_1 value of less than 0.02, confirming the reliability of the single-reference treatment by using B3LYP and CCSD(T) methods.[31]

All of the reported relative energies include ZPE correction. The DFT and QCISD(T) computations were carried out using the GAUSSIAN 98 program package.[32] All of the calculations were carried out on a DEC Alpha XP1000 1/500 professional workstation.

B. Calculation of Unimolecular Rate Constants. To evaluate the high-pressure-limit first-order rate constants from our quantum chemical calculations, the relation

$$k_\infty = \sigma(kT/h)\exp(\Delta S^{\ddagger}/R)\exp(-\Delta H^{\ddagger}/RT)$$

was used,[33,34] where h is the Planck constant, k is the Boltzmann factor, σ is the degeneracy of the reaction coordinate, and $\Delta H^{\ddagger}$ and $\Delta S^{\ddagger}$ are the enthalpy and entropy of activation, respectively. Since we deal with isomerizations, where there is no change in the number of moles, $\Delta H^{\ddagger} = \Delta E^{\ddagger}$, where $\Delta E^{\ddagger}$ is the energy difference between the transition state and the reactant. $\Delta E^{\ddagger}$ is equal to $\Delta E^{\circ}_{\text{total}} + \Delta(\text{ZPE})$, where $\Delta E^{\circ}_{\text{total}}$ is obtained by taking the difference between the total energies of the transition state and the reactant and Δ(ZPE) is the difference between the ZPEs of these species.

To estimate the tunneling effect in cases where H-atom migrations are an important component of the reaction coordinate, we used Wigner's inverted harmonic model,[35] where the tunneling effect $\Gamma(T)$ is given by

$$\Gamma(T) = 1 + \frac{1}{24}\left(\frac{h\nu^{\ddagger}}{kT}\right)^2 = 1 + \frac{1}{24}\left(\frac{hc\bar{\lambda}^{\ddagger}}{kT}\right)^2$$

and $\bar{\lambda}$ is the imaginary frequency of the reaction coordinate in cm^{-1}.[36]

In several cases, those involving H-atom migrations, as will be shown later, the imaginary frequencies were around 1200 cm^{-1}. For $T = 1100$ K and $\bar{\lambda} = 1226$ cm^{-1}, for example, the value of Γ is 1.107; namely, the tunneling correction is 10.7%. It is ~5% an 1600 K. These corrections are insignificant from both the accuracy of the calculations and the experimental results viewpoints. We therefore did not include any tunneling correction in our rate calculations. It should be mentioned that, at room temperature and lower, the tunneling effect must be taken into consideration but not at the temperatures of the shock tube regime.

Since the isomerization of indole has several products and its overall isomerization kinetics contains several parallel and consecutive steps, the comparison between the calculated apparent rate constants for the production of a given product and the experimental rates requires a modeling process. The computer modeling provides the concentrations of the reactant, products, and intermediates. The total isomerization rate constant is calculated from the relation

$$k_{\text{total}} = -\ln\{[\text{indole}]_t/[\text{indole}]_0\}/t$$

and the rate constant for the production of the given product is calculated from the relation

$$k_{\text{product}} = \frac{[\text{product}]_i}{[\text{indole}]_0 - [\text{indole}]_t}k_{\text{total}}$$

III. Results and Discussion

A. Tautomerization of Indole. As has been mentioned before, 3*H*-indole was suggested as an intermediate in the production of *o*- and *m*-tolunitrile from indole. Figure 1 shows the structures of the species that are involved in the tautomerization process of indole. Selected structural parameters of all the species on the potential energy surface are shown in Table 1, and the energetics at both B3LYP/cc-pVDZ//B3LYP/cc-pVDZ and CCSD(T)/cc-pVDZ//B3LYP/cc-pVDZ levels are shown in Table 2. 3*H*-Indole, the intermediate in the isomerization process, is ~5 kcal/mol less stable than indole, which is in agreement with the previously estimated value of 4.54 ± 2.39 kcal/mol. It is however considerably more stable than 2*H*-indole, which is ~24 kcal/mol less stable than indole. This ~19 kcal/mol difference in the stability of the 2*H*- and the 3*H*-tautomers can be attributed mainly to the loss of aromaticity of the benzene ring in the 2*H*-tautomer, where the two double

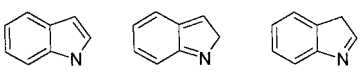

indole 2H-indole 3H-indole

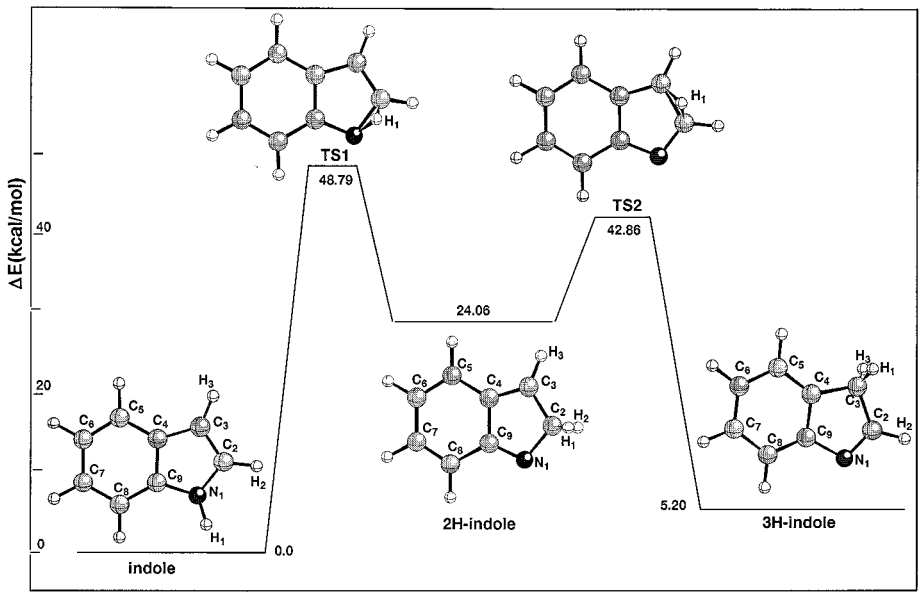

Figure 1. Potential energy profile of indole → 3*H*-indole tautomerization. Relative energies (kcal/mol) are calculated at the CCSD(T)//B3LYP/cc-pVDZ level of theory. Several geometrical parameters are shown in Table 1. The indole → 3*H*-indole tautomerization proceeds via an unstable tautomer, 2*H*-indole.

TABLE 1: Structural Parameters of Indole, 2*H*-Indole, and 3*H*-Indole and Transition States TS1 and TS2 Connecting These Tautomers[a]

param[b,c]	indole	TS1	2H-indole	TS2	3H-indole
r(N(1)−C(2))	1.383	1.467	1.456	1.364	1.290
r(C(2)−C(3))	1.374	1.411	1.499	1.435	1.515
r(C(3)−C(4))	1.439	1.407	1.363	1.411	1.506
r(C(4)−C(5))	1.409	1.424	1.442	1.420	1.391
r(C(5)−C(6))	1.391	1.377	1.363	1.379	1.400
r(C(6)−C(7))	1.413	1.430	1.454	1.429	1.402
r(C(7)−C(8))	1.392	1.378	1.362	1.378	1.400
r(C(8)−C(9))	1.402	1.420	1.448	1.423	1.394
r(C(4)−C(9))	1.426	1.440	1.483	1.443	1.410
r(N(1)−C(9))	1.380	1.362	1.306	1.354	1.423
r(N(1)−H(1))	1.100	1.353			
r(H(1)−C(2))		1.248	1.108		
r(H(2)−C(2))	1.087	1.091	1.108	1.092	1.095
r(H(1)−C(2))				1.253	
r(H(1)−C(3))				1.437	1.105
r(H(3)−C(3))	1.087	1.088	1.090	1.089	1.105

[a] Calculations were done at the B3LYP/cc-pVDZ level of theory. [b] Distances in angstroms. [c] The atom numbering is shown in Figure 1.

bonds are fixed in position in the ring. On the other hand, there is no loss of aromaticity in 3*H*-indole.

The bond distances obtained by the DFT calculations that are shown in Table 1 clearly point to the loss of aromaticity in 2*H*-indole. As can be seen all the bond distances in the benzene ring in indole and 3*H*-indole are roughly the same, whereas in 2*H*-indole the C(5)−C(6) and the C(7)−C(8) distances are approximately 1.36 Å (double bond), whereas the C(4)−C(5), C(6)−C(7), and C(8)−C(9) distances are approximately 1.44 Å (single bond).

The two transition states, TS1, which connects indole with 2*H*-indole, and TS2, which connects 2*H*-indole with 3*H*-indole, are very similar. The reaction coordinate in both cases is simply a 1,2-H-atom shift. The structures of the two transition states are close to the structure of 2*H*-indole. There is a complete loss of aromaticity of the benzene ring in the two transition states and in 2*H*-indole. A new double bond between C(9) and N(1) is formed at the expense of the double bond between C(2) and C(3) in the pyrrole ring (see Table 1).

The energy levels of the two transition states, above the ground state of indole, are 48.79 kcal/mol for TS1 and 42.86 kcal/mol for TS2. The energetics and geometrical characteristics of all the species on the potential energy surface are in agreement with the values of Smith and Liu,[11] who used the B3LYP/6-311++G(2d,2p)//B3LYP/6-31G* level of theory in their calculations. Our attempts to locate a transition state that directly connects indole with 3*H*-indole were unsuccessful, as were the attempts of Smith and Liu.[11]

B. Formation of *o*-*Tolunitrile.* *a. Potential Energy Surface Calculations.* We have not found any transition state connecting 2*H*-indole with any species, except 3*H*-indole. We have thus examined the potential energy surface connecting 3*H*-indole with the various isomers of indole. The potential energy surface of the 3*H*-indole → *o*-tolunitrile isomerization is shown in Figure 2. Several structural parameters of the species on the surface are shown in Table 3, and their energetics are shown in Table 2. The surface contains, in addition to 3*H*-indole and *o*-tolunitrile, two transition states and *o*-tolyl isocyanide as an intermediate.

The formation of *o*-tolyl isocyanide requires the rupture of the C(2)−C(3) bond and H-atom migration from C(2) to C(3). These two processes take place simultaneously; namely, *o*-tolyl isocyanide is formed via a concerted mechanism. The atom movement in the normal mode of the imaginary frequency in the transition state TS3 indicates that the reaction coordinate is a H(2)−N(1) stretch, which expresses itself also by a H(2)-C(2)N(1) angle bend. This angle changes from 121.96° to 151.43°. It leads to breaking of the C(2)−C(3) bond. The distance C(2)−C(3) changes from 1.515 Å in 3*H*-indole to 2.166 Å in TS3. In addition to the H(2)C(2)N(1) angle bend, there is a very big change in the dihedral angle H(2)C(2)N(1)C(9), from 180° to 23.13°, which brings the hydrogen atom H(1) close to C(3) to form a C(3)−H(1) bond in *o*-tolyl isocyanide. Although the C(2)−C(3) distance in the transition state TS3 is large, there are indications that the bond is not completely broken. First, it is a closed-shell singlet with no spin contamination (see Table 2), and second, there is substantial electron density between the two carbon atoms.

The energy barrier of the 3*H*-indole → *o*-tolyl isocyanide process, calculated at the coupled cluster (CCSD(T)) level of theory, is 77.49 kcal/mol, which is the highest energy level on the potential surface of the indole → *o*-tolunitrile isomerization.

TABLE 2: Total Energies E_{total} (au), Zero-Point Energies,[a] Relative Energies ΔE,[b] Imaginary Frequencies,[c] Entropies,[d] and Spin Contamination for All Species of Indole Isomerization, Calculated at the B3LYP/cc-pVDZ and CCSD(T)/cc-pVDZ// B3LYP/cc-pVDZ Computational Levels

	B3LYP						CCSD(T)	
species	E_{total}	ΔE[b]	ZPE[a]	S[d]	ν[c]	$\langle S^2 \rangle$	E_{total}	ΔE
				Reactant and Products				
indole	−363.842 320	0.00	79.62	79.19		0.0	−362.802 105	0.0
phenylacetonitrile	−363.823 705	10.11	78.05	88.92		0.0	−362.795 911	2.32
o-tolunitrile	−363.831 272	5.00	77.69	87.11		0.0	−362.802 729	1.53
m-tolunitrile	−363.830 628	5.30	77.58	88.98		0.0	−362.801 684	1.78
				Transition States and Intermediates				
TS1[e]	−363.757 227	50.22	76.44	78.32	(i-1440)	0.0	−362.719 282	48.79
2*H*-indole[e]	−363.794 606	28.76	78.44	79.67		0.0	−362.761 879	24.06
TS2[e]	−363.766 953	44.31	76.64	78.12	(i-1163)	0.0	−362.729 048	42.86
3*H*-indole[e]	−363.826 267	9.43	78.98	79.13		0.0	−362.792 796	5.20
TS3[f]	−363.699 016	85.10	74.80	82.57	(i-1226)	0.0	−362.662 713	82.64
o-tolyl isocyanide[f]	−363.798 278	25.26	77.28	87.06		0.0	−362.768 094	19.00
TS4[f]	−363.737 709	61.82	75.80	85.09	(i-381)	0.0	−362.709 662	54.19
TS5[g]	−363.673 964	101.26	75.24	83.91	(i-1219)	0.0	−362.639 532	97.64
TS6[h]	−363.750 939	55.15	77.43	78.46	(i-1319)	0.0	−362.712 999	53.72
INT1[h]	−363.773 467	41.91	78.32	79.71		0.0	−362.743 308	35.60
TS7[h]	−363.715 035	76.29	76.04	80.73	(i-509)	0.52	−362.679 487	73.36
INT2[h]	−363.738 248	61.95	76.26	85.64		1.03	−362.694 904	63.91
TS8[h]	−363.705 851	79.83	73.81	85.88	(i-1315)	0.37	−362.669 358	77.49

[a] Zero-point energies in kcal/mol. ZPEs were scaled by the ZPE scaling factor of 0.9806.[18] [b] Relative energies in kcal/mol. $\Delta E = \Delta E_{total} + \Delta(ZPE)$. [c] Imaginary frequencies in cm^{-1}. [d] Entropies in cal/(K·mol). Entropies were scaled by the entropy scaling factor of 1.0015.[18] [e] See Figure 1. [f] See Figure 2. [g] See Figure 7. [h] See Figures 8 and 9.

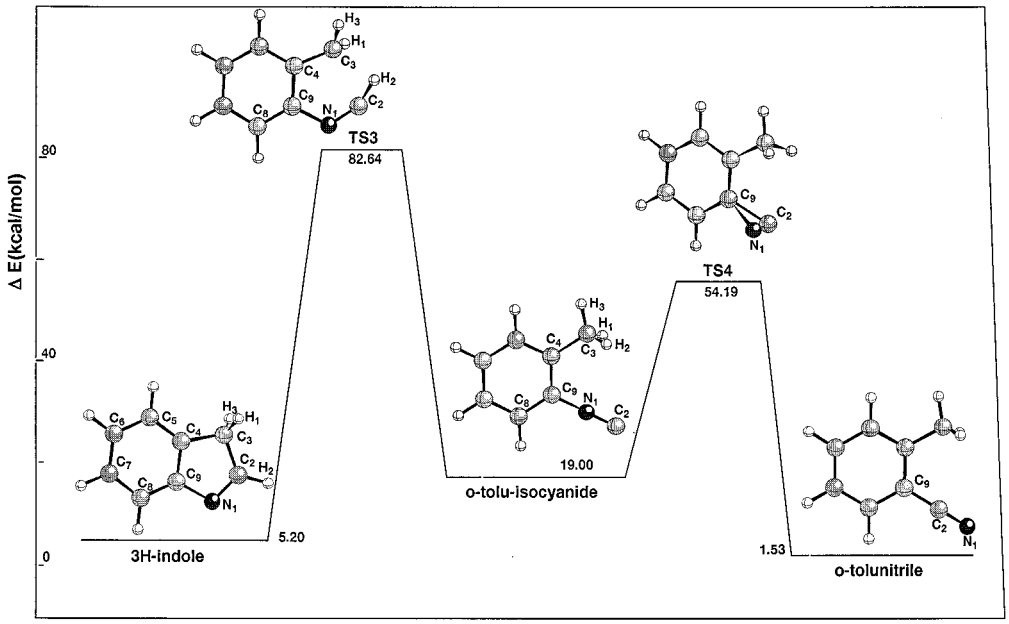

Figure 2. Potential energy profile of 3*H*-indole → *o*-tolunitrile isomerization. Relative energies (kcal/mol) are calculated at the CCSD(T)//B3LYP/cc-pVDZ level of theory. Several geometrical parameters are shown in Table 3. The isomerization proceeds via *o*-tolyl isocyanide that by −NC → −CN flip forms *o*-tolunitrile.

The energy level of *o*-tolyl isocyanide is 19.0 kcal/mol higher than that of indole and 17.47 kcal/mol above that of *o*-tolunitrile at the CCSD(T) level of theory (see Table 2).

The final stage in the reaction is *o*-tolyl isocyanide → *o*-tolunitrile rearrangement via TS4. The structure of the transition state TS4 is similar to the structures of other R−NC → R−CN rearrangements.[37,38] The reaction coordinate is a rotation of the N−C group, which leads to C(9)−N(1) bond breaking simultaneously with C(9)−C(2) bond formation. The N(1)−C(9) distance changes from 1.390 Å in *o*-tolyl isocyanide to 1.818 Å in TS4, and a new bond, C(9)−C(2), with a length of 1.644 Å is formed. In *o*-tolunitrile, the N(1)−C(9) bond is completely broken and C(2)−C(9) changes from 1.644 to 1.437 Å. In addition, the C(9)C(2)N(1) angle changes from 78° to 180°.

The energy barrier of this stage is 48.99 kcal/mol above the 3*H*-indole level. The energy barrier for *o*-tolyl isocyanide → *o*-tolunitrile rearrangement itself is only 35.19 kcal/mol calculated at the CCSD(T) level of theory. The value of 35.19 kcal/mol agrees with values of ∼38.5 kcal/mol derived from the results of a kinetic study on various R−NC → R−CN rearrangements using photoelectron spectroscopy[38] and with a value of 35.0 kcal/mol calculated at the QCISD(T)/6-311G**// B3LYP/6-31G** level of theory.[5] It is also in excellent

TABLE 3: Structural Parameters of All Species of the Reaction 3*H*-Indole → *o*-Tolunitrile Calculated at the B3LYP/cc-pVDZ Level of Theory

param[a,b]	3*H*-indole	TS3	*o*-tolyl isocyanide	TS4	*o*-tolunitrile
r(N(1)−C(2))	1.290	1.234	1.183	1.202	1.165
r(C(2)−C(3))	1.515	2.166			
r(C(3)−C(4))	1.506	1.468	1.505	1.502	1.507
r(C(4)−C(5))	1.391	1.404	1.401	1.402	1.400
r(C(5)−C(6))	1.400	1.399	1.398	1.398	1.399
r(C(6)−C(7))	1.402	1.401	1.398	1.399	1.398
r(C(7)−C(8))	1.400	1.397	1.394	1.394	1.394
r(C(8)−C(9))	1.394	1.395	1.402	1.400	1.406
r(C(4)−C(9))	1.430	1.418	1.412	1.410	1.416
r(N(1)−C(9))	1.423	1.417	1.390	1.818	
r(C(2)−C(9))				1.644	1.437
∠(C(9)C(2)N(1))				77.70	179.48

[a] Distances in angstroms. [b] The atom numbering is shown in Figure 2.

agreement with a value of 38.4 kcal/mol obtained in the single-pulse shock tube experiments on the $CH_3NC \rightarrow CH_3CN$ isomerization.[39,40] Similar results were obtained recently by Zhou and Liu[12] at the B3LYP/6-311++G(2d,2p)//B3LYP/6-31G** level.

We have calculated the dipole moment of the species on the potential energy surface of 3*H*-indole → *o*-tolunitrile isomerization and found the following values: 2.26, 1.65, 3.66, 2.79, and 4.06 D for 3*H*-indole, TS3, *o*-tolyl isocyanide, TS4, and *o*-tolunitrile, respectively. In addition, the charge distribution in the isocyanide, calculated using the CHELPG (grid-oriented charges from electrostatic potentials) method,[41] is +0.45 on N(1) and −0.43 on C(8). In the nitrile, the picture is reversed and the charge is −0.44 on the nitrogen atom and +0.35 on C(8). This charge distribution is the reason for the high dipole moment of *o*-tolyl isocyanide and *o*-tolunitrile.

b. Calculation of the Isomerization Rate Constant. The rate of formation of *o*-tolunitrile was calculated by computer modeling as described in section II, using the reaction scheme that is shown in Table 4. The table contains the species and the rate parameters of the steps on all the potential energy surfaces. The value obtained for the apparent rate constant of the indole → *o*-tolunitrile reaction is $k(\text{indole} \rightarrow o\text{-tolunitrile}) = 10^{11.46}T \exp(-84.87 \times 10^3/RT)$. Figure 3 shows a comparison between the calculated and experimentally obtained rate constants. As can be seen the calculated value is about a factor of 6 below the experimental points. This corresponds to a 4.5 kcal/mol difference in the energy barrier at 1250 K, which can be considered satisfactory.

A sensitivity analysis shows that the production rate of *o*-tolunitrile is solely dependent on the rate constant of reaction 3, 3*H*-indole → *o*-tolyl isocyanide (Table 4), as this is the slowest reaction in the sequence indole → 2*H*-indole → 3*H*-indole → *o*-tolyl isocyanide → *o*-tolunitrile. The yield of *o*-tolunitrile depends linearly on k_3.

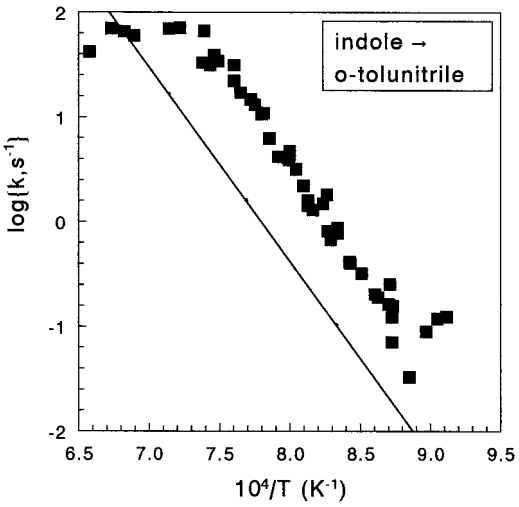

Figure 3. An Arrhenius plot of the calculated apparent rate constant of indole → *o*-tolunitrile isomerization obtained by computer modeling of the indole isomerization scheme (Table 4). The experimental data are presented as full squares in the figure. The calculated rate constant somewhat underestimates the isomerization rate. The disagreement corresponds to a 4.5 kcal/mol difference in the reaction barrier.

C. Formation of *m*-Tolunitrile. As a first trial, we assumed that *o*-tolyl isocyanide, which is the intermediate in indole → *o*-tolunitrile isomerization, would be the precursor of *m*-tolunitrile too. In this case, the C(3)−C(2) bond breaking is accompanied by a C(8)−N(1) bond formation rather than a C(9)−N(1) bond formation as in *o*-tolunitrile (Figure 2). The main difference, however, between the formations of *o*-tolunitrile and *m*-tolunitrile is that the latter requires, in addition to the −NC → −CN flip, a hydrogen atom migration from the *meta* to the *ortho* position. If the −NC → −CN flip and the H-atom migration do not occur as a single, concerted process, a biradical or a carbene must be formed as an intermediate. We found a reaction path that involves two transition states and one intermediate that has a carbene structure. This is shown in Figure 4a. However, the highest point on the surface that described the process is very high and is not compatible at all with the experimental observations.

As a second trial, we used *o*-tolunitrile as a starting species rather than *o*-tolyl isocyanide. The reaction path for this process is shown in Figure 4b. On the potential surface of this path there are again two transition states and one intermediate with a carbene structure, where the H atom has migrated from the *meta* to the *ortho* position. Here the highest point on the surface is somewhat lower than the highest point in the previous path,

TABLE 4: Reaction Scheme for the Isomerization of Indole

	reaction	σ[a]	$\Delta S^{\ddagger}$[b]	A[c]/T	E_a[d]	$\Delta S°_{reaction}$[e]	$\Delta H°_{reaction}$[f]
1	indole → 2*H*-indole	1	−0.87	1.3×10^{10}	48.8	0.48	24.1
2	2*H*-indole → 3*H*-indole	2	−1.55	1.9×10^{10}	18.8	1.01	−18.9
3	3*H*-indole → *o*-tolyl isocyanide	1	3.44	1.2×10^{11}	77.4	7.93	13.8
4	*o*-tolyl isocyanide → *o*-tolunitrile	1	−1.97	7.7×10^{9}	35.2	0.05	−17.5
5	*o*-tolunitrile → INT	1	−0.38	1.7×10^{10}	95.3	2.41	89.0
6	INT → *m*-tolunitrile	1	−1.80	8.4×10^{8}	9.17	−0.54	−87.5
7	indole → INT1	1	−0.73	1.4×10^{10}	53.7	0.52	36.6
8	INT1 → INT2	1	1.02	3.5×10^{10}	37.8	5.93	28.3
9	INT2 → phenylacetonitrile	1	0.24	2.4×10^{10}	13.6	3.28	61.6

[a] Reaction coordinate degeneracy. [b] Entropy of activation in cal/(K·mol). [c] Preexponential factor in s^{-1}. [d] Activation energy in kcal/mol. [e] Entropy of reaction in cal/(K·mol). [f] Enthalpy of reaction in kcal/mol.

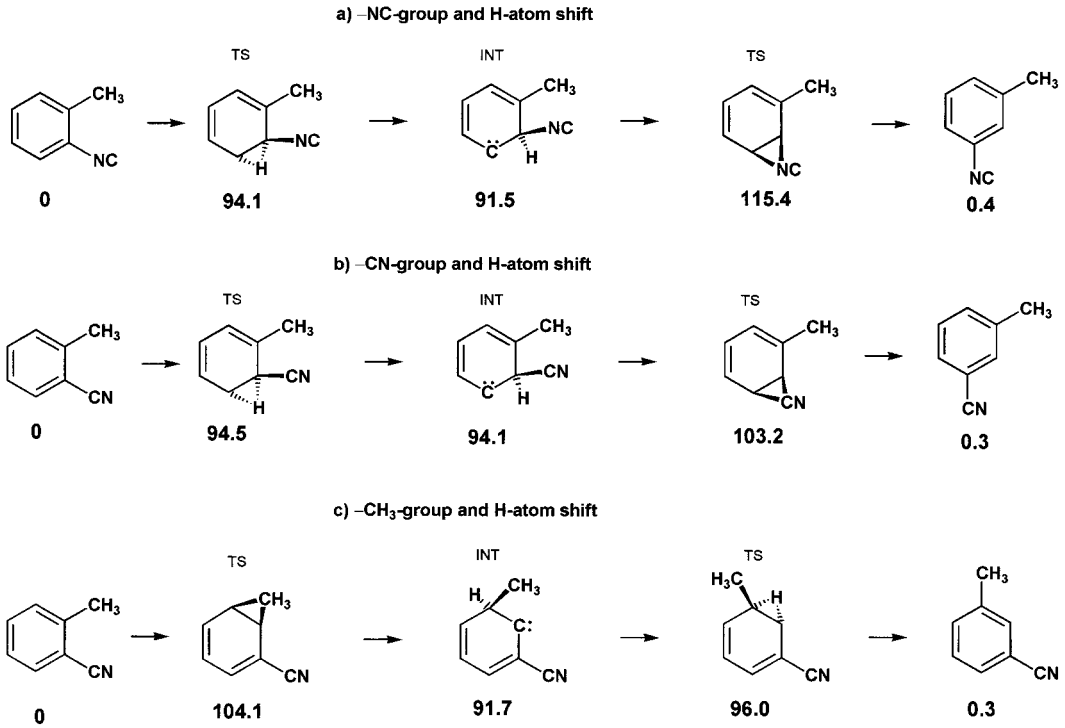

Figure 4. Three reaction pathways for the formation of *m*-tolunitrile. Relative energies (kcal/mol) are calculated at the B3LYP/cc-pVDZ level of theory. The very high activation energies in the three pathways are incompatible with the experimental findings.[1]

103.2 kcal/mol compared to 115.4 kcal/mol, calculated at the B3LYP/cc-pVDZ//B3LYP/ cc-pVDZ level of theory.

The third trial was an attempt to move a methyl group from the *ortho* to the *meta* position and a hydrogen atom from the *meta* to the *ortho* position. This path is shown in Figure 4c. The highest point on this surface is 104.1 kcal/mol.

As reaction path b has the lowest energy, we performed CCSD(T)/cc-pVDZ// B3LYP/cc-pVDZ calculations for this path and calculated the rate constants of reactions 5 and 6 as shown in Table 4. An apparent isomerization rate constant for the reaction indole → *m*-tolunitrile as obtained by the computer modeling is $k(\text{indole} \rightarrow m\text{-tolunitrile}) = 10^{23.03}T \exp(-181.15 \times 10^3/RT)$. This value of the apparent rate constant does not correspond to a single rate constant but rather to a combination of rate constants and probably an equilibrium constant in which high activation energies and heats of reaction are involved. In any case, the comparison between the calculated apparent rate constant and the experimental rates as shown in Figure 5 gives very poor agreement. We believe that one of the reasons that the calculated rate constant is lower by more than a factor of 10^4 (at 1250 K, for example) is the fact that the path goes through *o*-tolunitrile, whose concentration, at least at the low end of the experimental temperature range, is very low. It is suggested that the three possible pathways described in this section cannot represent the pathway for the formation of *m*-tolunitrile.

As a second option, we assumed that isomerization occurs not from indole, but from indole radical after losing a hydrogen atom, most probably by abstraction processes. We have thus calculated the potential energy surfaces for three pathways starting from radical structures of either *o*-tolunitrile or *o*-tolyl isocyanide. Two radicals that served as starting points were obtained by removing hydrogen atom from the benzene ring and one from the methyl group. The three pathways are shown in Figure 6, and the values in the figure are calculated at the B3LYP/cc-pVDZ level of theory. As can be seen, particularly in path b, the highest point is low, only 40 kcal/mol. Of course,

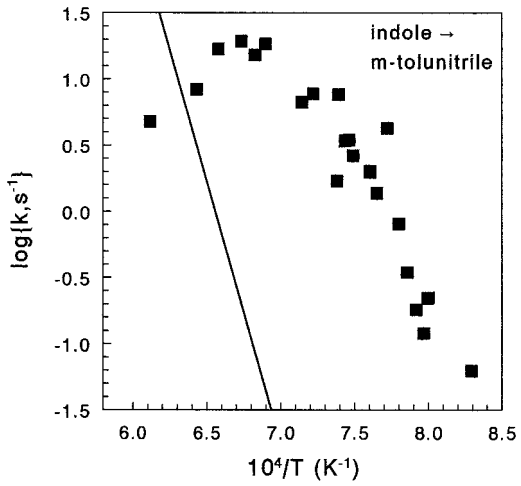

Figure 5. An Arrhenius plot of the calculated apparent rate constant of indole → *m*-tolunitrile isomerization obtained by computer modeling of the indole isomerization scheme (Table 4). The experimental data are presented as full squares in the figure. The calculated rate constant is several orders of magnitude below the experimental rates, indicating that this path cannot represent the formation of *m*-tolunitrile.

the apparent rate of appearance highly depends on the initial concentration of the radical. Since this concentration depends on several abstraction reactions, we cannot compare a calculated rate constant based on the data in Figure 6b to the experimental results. We believe, however, that the formation of *m*-tolunitrile does not proceed directly from indole, but from a radical species.

D. Formation of Phenylacetonitrile. It has been shown that the pyrrole → vinylacetonitrile isomerization proceeds only via a 2*H*-pyrrole intermediate. We have assumed that the equivalent reaction in indole, indole → phenylacetonitrile, proceeds in a similar manner, namely, via 3*H*-indole. However, we looked for additional reaction channels, which are isomerizations directly from indole and via 2*H*-indole as an intermediate.

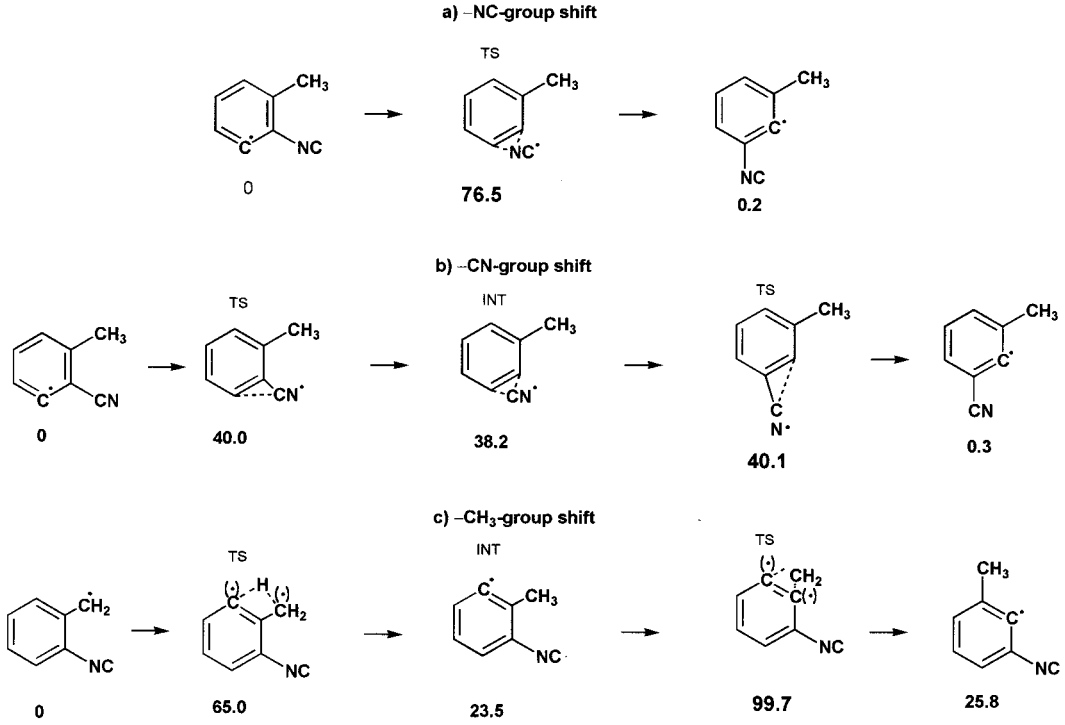

Figure 6. Three reaction pathways for the formation of *m*-tolunitrile starting from radical species. Relative energies (kcal/mol) are calculated at the B3LYP/cc-pVDZ level of theory. Much lower activation energies appear in these pathways. It is believed that the radical species that are formed by various abstraction reactions are responsible for this isomerization process.

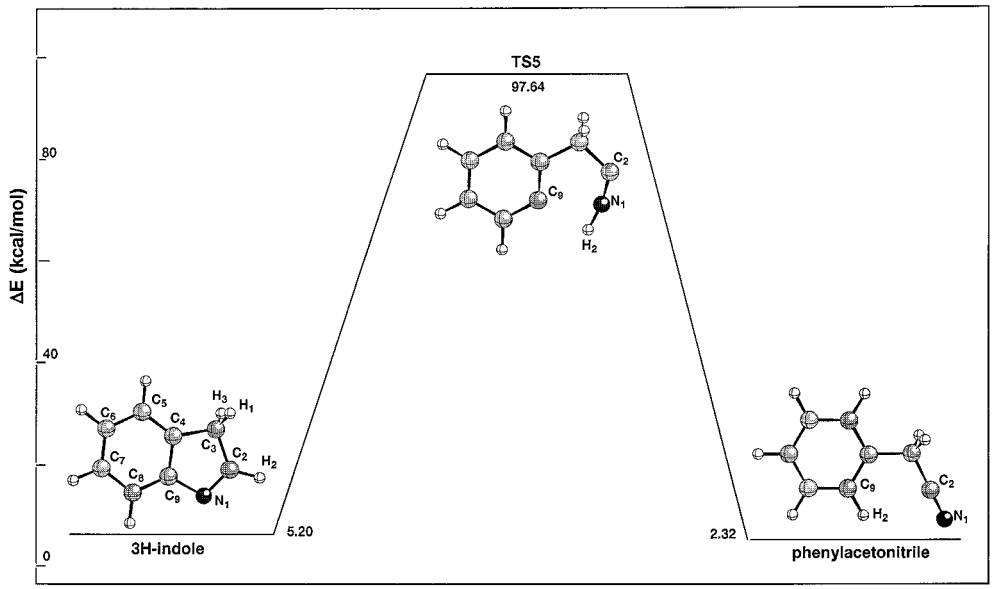

Figure 7. Potential energy profile of 3*H*-indole → phenylacetonitrile isomerization. Relative energies (kcal/mol) are calculated at the CCSD(T)//B3LYP/cc-pVDZ level of theory. In view of the very high activation energy on the surface, this reaction path is insignificant from a kinetics viewpoint (see also Figure 8).

Whereas the potential energy surfaces from indole to phenylacetonitrile and from 3*H*-indole to phenylacetonitrile were established, we could not locate any transition state leading to phenylacetonitrile from 2*H*-indole.

a. 3H-Indole → Phenylacetonitrile Pathway. The potential energy surface of 3*H*-indole → phenylacetonitrile is shown in Figure 7. This reaction has a concerted mechanism, where the C(9)−N(1) bond in the transition state TS5 (2.185 Å) is broken and H(1) moves from C(2) to N(1). Although this potential surface is very simple in the sense that there are no intermediates and there is only one transition state, the isomerization barrier of 97.64 kcal/mol at the CCSD(T) level of theory is very high compared to that of the direct isomerization from indole as will be shown later. In view of the high barrier, this reaction path is insignificant from a kinetic viewpoint.

b. Indole → Phenylacetonitrile Pathway. The potential energy surface of the direct indole → benzyl cyanide isomerization, not involving 3*H*-indole, is shown in Figure 8, and the detailed reaction path and the structures of the species on the surface are shown in Figure 9. Selected structural parameters of the species on the surface are shown in Table 5, and the energetics at both the B3LYP/cc-pVDZ//B3LYP/cc-pVDZ and CCSD(T)/cc-pVDZ//B3LYP/ cc-pVDZ levels of theory are shown in Table 2.

The potential energy surface contains three transition states and two intermediates. The first stage in the process is the

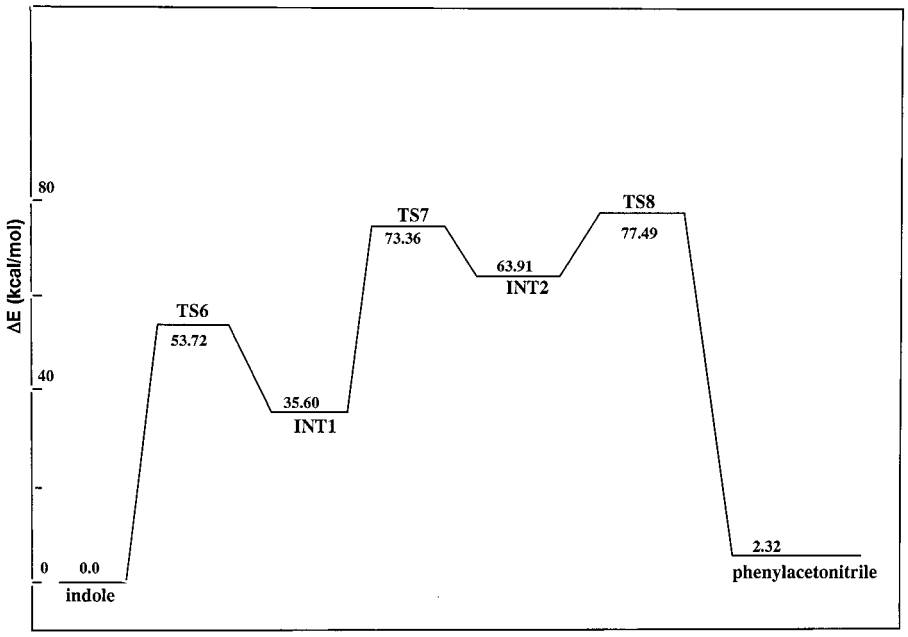

Figure 8. Potential energy surface of indole → phenylacetonitrile isomerization. Relative energies (kcal/mol) are calculated at the CCSD(T)//B3LYP/cc-pVDZ level of theory. Much lower activation energies appear on this surface as compared to that of the direct isomerization of indole.

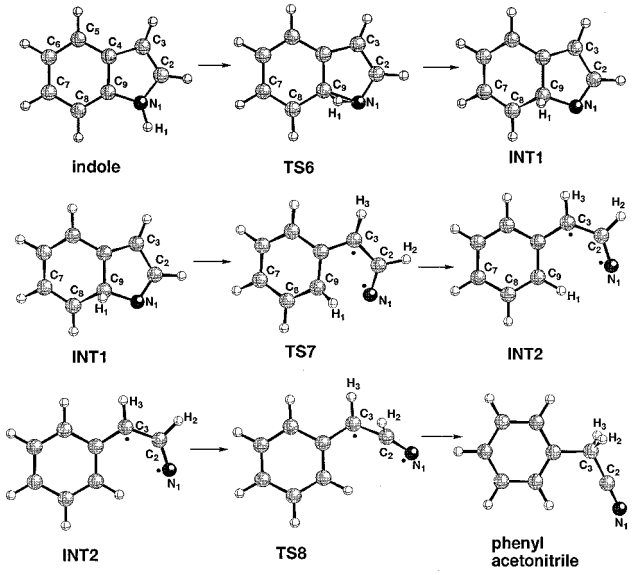

Figure 9. Details of the reaction pathways and the species involved in the surface shown in Figure 8. Several geometrical parameters are shown in Table 5.

movement of H(1) from the nitrogen atom to C(9) via transition state TS6 to form the intermediate INT1. This step resembles to some extent the tautomerization from indole to 2*H*-indole in the sense that the hydrogen atom moves from the nitrogen to an adjacent carbon atom except that the shift is to C(9) and not C(2) as in the tautomerization. In both cases, the two remaining double bonds in the benzene rings are fixed, causing loss of aromaticity. The reaction coordinate of TS6 is simply a 1,2-H-atom shift from N(1) to C(9), and the energy barrier for the process is 53.72 kcal/mol.

It is interesting to compare the structure and energetics of 2*H*-indole to those of INT1 as both of them are obtained by a 1,2-H-atom shift in indole from the nitrogen to an adjacent carbon atom. The relatively high energy of INT1 (35.60 kcal/mol at the CCSD(T) level of theory) compared to that of 2*H*-indole (24.06 kcal/mol) is probably the result of the distortion in the angles N(1)C(9)H(1) (101.7°) and C(8)C(9)H(1) (103.3°)

TABLE 5: Several Structural Parameters of All Species of the Reaction Indole → Phenylacetonitrile, Calculated at the B3LYP/cc-pVDZ Level of Theory

param[a,b]	indole	TS6	INT1	TS7	INT2	TS8	phenyl-acetonitrile
r(N(1)−C(2))	1.383	1.357	1.301	1.283	1.273	1.212	1.161
r(C(2)−C(3))	1.374	1.402	1.461	1.443	1.447	1.451	1.466
r(C(3)−C(4))	1.439	1.406	1.366	1.396	1.426	1.437	1.525
r(C(4)−C(5))	1.409	1.422	1.441	1.432	1.424	1.418	1.403
r(C(5)−C(6))	1.391	1.378	1.364	1.377	1.389	1.391	1.395
r(C(6)−C(7))	1.413	1.433	1.460	1.426	1.403	1.402	1.399
r(C(7)−C(8))	1.392	1.373	1.353	1.383	1.403	1.401	1.396
r(C(8)−C(9))	1.402	1.439	1.498	1.417	1.390	1.391	1.399
r(C(4)−C(9))	1.426	1.450	1.507	1.446	1.423		1.399
r(N(1)−C(9))	1.380	1.465	1.461	2.215	3.009		
r(N(1)−H(1))	1.100	1.393					
r(H(1)−C(9))		1.233	1.119	1.093	1.092		
r(H(2)−C(2))	1.087	1.091	1.096	1.107	1.112	1.200	1.104
r(H(2)−C(3))						1.726	1.104

[a] Distances in angstroms. [b] The atom numbering is shown in Figure 9.

from the characteristic sp^3 value of ∼112° in 2*H*-indole. Another major difference between 2*H*-indole and INT1 is the loss of the planarity in INT1. Whereas the dihedral angle C(2)N(1)-C(9)C(8) in 2*H*-indole is 180°, the same angle in INT1 is 141°.

The transition from INT1 to INT2 proceeds via transition state TS7 (Figure 9). The reaction coordinate of transition state TS7 is a double rotation of the N(1)C(2)H(2) group with respect to the H(1)C(9)C(8) group. As a result of the rotation, the C(9)−N(1) bond extends from a distance of 1.416 Å in INT1 to 2.215 Å in the transition state TS7 and further to 3.009 Å in INT2. The intermediate INT2 is a planer biradical (open-shell singlet) with a spin contamination, $\langle S^2 \rangle$, of 1.03. The transition state TS7 is partially biradical with $\langle S^2 \rangle = 0.52$. The dihedral angle H(1)C(9)C(8)C(7) in INT1 is 90.70°. It is 150.29° in TS7 and 180° in INT2.

The ground-state energy of INT2 at the CCSD(T) level of theory is 63.91 kcal/mol above that of indole and 28.31 kcal/mol above the ground-state energy of INT1. The small energy difference between INT2 and INT1 although a C−N bond is broken can be rationalized by the regain of aromaticity in INT2

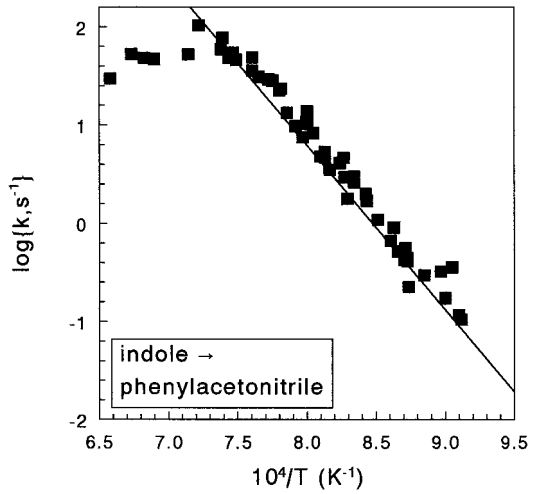

Figure 10. An Arrhenius plot of the calculated apparent rate constant of indole → phenylacetonitrile isomerization obtained by computer modeling of the indole isomerization scheme (Table 4). The experimental data are presented as full squares in the figure. The agreement is excellent.

and the release of a large amount of strain energy which exists in INT1. The energy level of TS7 is 73.36 kcal/mol relative to that of indole, but only 37.76 kcal/mol above that of INT1 (Figure 8) as some of the strain energy in INT1 is already released in TS7. However, aromaticity has not yet been gained in the transition state.

The final stage in the indole → phenylacetonitrile isomerization is a 1,2-H-atom shift from C(2) to C(3) in INT2 via transition state TS8. The bond of H(2)−C(2) in the transition state is only slightly stretched from 1.112 Å in INT2 to 1.200 Å in TS8. However, the H(2)C(2)C(3) angle decreases from 115.24° to 80.60°, and the dihedral angle H(2)C(2)C(3)C(4) decreases from 180° to 98.81°. In addition, the bond N(1)−C(2) (1.273 Å) in INT2, which is a double bond, is shortened to a value of 1.212 Å in TS8, which is closer to a triple bond. The C≡N bond length in phenylacetonitrile is 1.161 Å. The transition state TS8 still retains some of the spin contamination of INT2. It is $\langle S_{TS8}^2 \rangle = 0.37$ compared to $\langle S_{INT2}^2 \rangle = 1.03$. The spin contamination in TS8 disappears completely in phenylacetonitrile.

The energy of the transition state TS8 calculated at the CCSD(T) level of theory is 77.49 kcal/mol above the ground-state energy of indole, and it is the highest point on the indole → phenylacetonitrile potential energy surface. However, the barrier of the INT2 → phenylacetonitrile step is only 13.58 kcal/mol, which is considerably less than normal barriers of the 1,2-H-atom shift in closed-shell species.

c. Calculation of the Isomerization Rate Constant. As can be seen in Figure 8, there are three transition states on the potential energy surface of the indole → phenylacetonitrile isomerization. The three reactions corresponding to the three transition states are reactions 7−9 in Table 4. The rate constant for the formation of phenylacetonitrile from indole as obtained by the computer modeling is given by k(indole → phenylacetonitrile) = $10^{11.19}T \exp(-76.59 \times 10^3/RT)$. It is shown in comparison with the experimental rates in Figure 10. The agreement is excellent. A sensitivity analysis shows that the production rate of phenylacetonitrile is dependent solely on reaction 8.

IV. Conclusions

The isomerization of indole can be summarized by the following features.

(1) *o*-Tolunitrile is formed via the stable tautomer 3*H*-indole. The mechanism of the tautomerization is two consecutive 1,2-H-atom shifts in the five-membered ring. The isomerization of 3*H*-indole to *o*-tolunitrile proceeds via *o*-tolyl isocyanide, which by −NC → −CN rearrangement forms *o*-tolunitrile.

(2) Phenylacetonitrile is formed directly from indole via a reaction path that contains three transition states and two intermediates. A reaction path via 3*H*-indole has a very high barrier and does not contribute to the overall rate of the isomerization process.

(3) *m*-Tolunitrile formation from *o*-tolunitrile and *o*-tolyl isocyanide has very high barriers on the potential surface owing to the formation of highly energetic carbene structures both in the intermediates and in the transition states. These reaction pathways cannot describe the isomerization of indole to *m*-tolunitrile. On the other hand, a potential surface, where the starting point is a radical, shows low-energy barriers for the formation of *m*-tolunitrile. On the basis of these observations, it is suggested that indole radicals, which are formed by various abstraction reactions, are possible precursors for the formation of *m*-tolunitrile.

(4) A reaction scheme containing nine elementary steps taken from the various reaction paths of indole isomerization was used to calculate, by computer modeling, apparent rate constants for product formation. The agreement between the calculated values and the experimental rate data is very good.

Acknowledgment. We thank the Ministry of Absorption for a fellowship to F.D. in the frame of the Giladi program.

References and Notes

(1) Laskin, A.; Lifshitz, A. *J. Phys. Chem. A* **1997**, *101*, 7787.
(2) Lifshitz, A.; Tamburu, C.; Suslensky, A. *J. Phys. Chem. A* **1989**, *93*, 5802.
(3) Mackie, J. C.; Colket, M. B., III; Nelson, P. F.; Esler, M. *Int. J. Chem. Kinet.* **1991**, *23*, 733.
(4) Martoprawiro, M.; Bacskay, G. B.; Mackie, J. C. *J. Phys. Chem. A* **1999**, *103*, 3923.
(5) Zhai, L.; Zhou, X.; Liu, R. *J. Phys. Chem. A* **1999**, *103*, 3917.
(6) Dubnikova, F.; Lifshitz, A. *J. Phys. Chem. A* **1998**, *102*, 10880.
(7) Gut, I. G.; Wirz, J. *Angew. Chem., Int. Ed. Engl.* **1994**, *33*, 1153.
(8) Collier, W. B.; Magdo, I.; Klots, T. D. *J. Chem. Phys.* **1999**, *110*, 5710.
(9) El-Azhary, A. A. *Specrochim. Acta, A* **1999**, *55*, 2437.
(10) Walden, S. E.; Wheeler, R. A. *J. Chem. Soc., Perkin Trans.* **1996**, 2653.
(11) Smith, B. J.; Liu, R. *J. Mol. Struct.: THEOCHEM* **1999**, *491*, 211.
(12) Zhou, X.; Liu, R. *J. Mol. Struct.: THEOCHEM* **1999**, *461−462*, 569.
(13) Becke, A. D. *J. Chem. Phys.* **1993**, *98*, 5648.
(14) Lee, C.; Yang, W.; Parr, R. G. *Phys. Rev.* **1988**, *B37*, 785.
(15) Dunning, T. H., Jr.; Fabian, J. *Eur. J. Org. Chem.* **1999**, *1107*, 7.
(16) Schlegel, H. B. *J. Comput. Chem.* **1982**, *3*, 214
(17) Peng, C.; Schlegel, H. B. *Isr. J. Chem.* **1993**, *33*, 449.
(18) Scott, A. P.; Radom, L. *J. Phys. Chem.* **1996**, *100*, 16502.
(19) Shaik, S. S.; Schlegel, H. B.; Walfe, S. *Theoretical Aspects of Physical Organic Chemistry the SN2 Mechanism*; Wiley: New York, **1992**; p 45.
(20) Sperling, D.; Reissig, H.-U.; Fabian, J. *Eur. J. Org. Chem.* **1999**, *1107*, 7.
(21) Sperling, D.; Fabian, J. *Eur. J. Org. Chem.* **1999**, *215*, 5.
(22) Houk, K. N.; Nendel, M.; Wiest, O.; Storer, J. M. *J. Am. Chem. Soc.* **1997**, *101*, 1095.
(23) Fan, K.-N.; Li, Z.-H.; Wang, W.-N.; Huang, H.-H.; Huang, W. *Chem. Phys. Lett.* **1997**, *277*, 257.
(24) Skancke, P. N.; Hrovat, D. A.; Borden, W. T. *J. Phys. Chem.* **1999**, *103*, 4043.
(25) Goddard, J. D.; Orlova, G. *J. Chem. Phys.* **1999**, *111*, 7705.
(26) Hess, B. A., Jr.; Eckart, U.; Fabian, J. *J. Am. Chem. Soc.* **1998**, *120*, 12310.
(27) Brinck, T.; Lee, H.-N.; Jonsson, M. *J. Phys. Chem.* **1999**, *103*, 7094.
(28) Scuseria, G. E.; Schaefer, H. F., III. *J. Chem. Phys.* **1989**, *90*, 3700.
(29) Pople, J. A.; Head-Gordon, M.; Raghavarchari, K.; Trucks, G. W. *Chem. Phys. Lett.* **1987**, *87*, 5968.

(30) Lee, T. J.; Taylor, P. R. *Int. J. Quantum Chem. Symp.* **1989**, *23*, 199.
(31) Lee, T. J.; Rendell, A. P.; Taylor, P. R. *J. Phys. Chem.* **1990**, *94*, 5463.
(32) Frisch, M. J.; Trucks, G. W.; Schlegel, H. B.; Scuseria, G. E.; Robb, M. A.; Cheeseman, J. R.; Zakrzewski, V.G.; Montgomery, J. A., Jr.; Stratmann, R. E.; Burant, J. C.; Dapprich, S.; Millam, J. M.; Daniels, A. D.; Kudin, K. N.; Strain, M. C.; Farkas, O.; Tomassi, J.; Barone, V.; Cossi, M.; Cammi, R.; Mennucci, B.; Pomelli, C.; Adamo, C.; Clifford, S.; Oshterski, J.; Petersson, G. A.; Ayala, P. Y.; Cui, Q.; Morokuma, K.; Malick, D. K.; Rabuck, A. D.; Rahavachari, K.; Foresman, J.B.; Cioslowski, J.; Orviz, J. V.; Baboul, A. G.; Stefanov, B. B.; Liu, G.; Liashenko, A.; Piskorz, P.; Komarini, I.; Gomperts, R.; Martin, R. L.; Fox, D. J.; Keith, T.; Al-Laham, M. A.; Peng, C. Y.; Nanayakkara, A.; Gonzalez, C.; Challacombe, M.; Gill, P. M. W.; Johnson, B.; Chen, M. W.; Wong, M. W.; Andres, J. L.; Head-Gordon, M.; Replogle, E. S.; Pople, J. A. *GAUSSIAN 98*, Revision A.7; Gaussian, Inc.: Pittsburgh, PA, 1998.
(33) Eyring, H. *J. Chem. Phys.* **1935**, *3*, 107.
(34) Evans, M. G.; Polanyi, M. *Trans. Faraday Soc*. **1935**, *31*, 875.
(35) Wigner, E. *Z. Phys. Chem.* **1932**, *B19*, 203.
(36) Louis, F.; Gonzales, C. A.; Huie, R.; Kurylo, M. J. *J. Chem. Phys. A* **2000**, *104*, 8773.
(37) Ruchardt, C.; Meier, M.; Haaf, K.; Pakusch, J.; Wolber, E. K. A.; Muller, B. *Angew. Chem.* **1991**, *30*, 893.
(38) Wang, D.; Qian, X.; Zhang, Q. *Chem. Phys. Lett.* **1997**, *266*, 560.
(39) Schneider, F. W.; Rabinovitch, B. S. *J. Am. Chem. Soc*. **1963**, *85*, 2365.
(40) Lifshitz, A.; Carroll, H. F.; Bauer, S. H. *J. Am. Chem. Soc.* **1964**, *86*, 1488.
(41) Breneman, C. M.; Wiberg, K. B. *J. Comput. Chem.* **1990**, *11*, 361.